Bounded Input Dissipativity of Linearized Circuit Models

Bounded Input Dissipativity of Linearized Circuit Models

Tommaso Bradde, *Student Member, IEEE*, Stefano Grivet-Talocia, *Fellow, IEEE*, Giuseppe C. Calafiore, *Fellow, IEEE*, Anton V. Proskurnikov, *Senior Member, IEEE*, Zohaib Mahmood, Luca Daniel, *Senior Member, IEEE*

***Abstract*—We introduce the concept of Bounded Input Dissipativity (BID) for the characterization from an energy perspective of linearized models of nonlinear circuit blocks. Such linearized models are commonly employed in the design of large systems to approximate circuit blocks that operate in the neighborhood of some well-defined and asymptotically stable bias point and lead to a dramatic reduction in circuit simulation runtime. Even if the original circuit block always behaves as a dissipative system, its linearized model may behave as dissipative or non-dissipative depending on the amplitude of its small-signal port voltages and currents, compared to the corresponding constant bias or supply signal components. This paper presents a theoretical framework for the analysis of such a conditional dissipativity and introduces BID criteria based on the feasibility of Bilinear or Linear Matrix Inequalities. These criteria allow to estimate the maximum small-signal input amplitude that guarantees the dissipativity of the linearized model. Various examples demonstrate the validity of the proposed theory, including a test case showing how spurious and physically inconsistent instabilities may arise if the proposed BID conditions are not verified.**

I. Introduction and motivations

Dissipative systems [1]–[6] are unable to generate energy on their own and can only deliver power if some energy has been previously stored in them. It is well known that, under proper technical assumptions, interconnections of dissipative systems are dissipative [4] and stable [7]. These two aspects have motivated strong interest and numerous efforts during the last few decades aimed at the characterization and enforcement of dissipativity in simulation models, especially in the Signal and Power Integrity communities [8], [9]. Numerical simulations based on dissipative models are guaranteed to be reliable and robust, whereas the presence of even one single non-dissipative model, able to indefinitely supply power to its environment, may lead to oscillations and instabilities. In the particular case of linear systems, the dissipativity conditions can be expressed and verified in several convenient ways, including Linear Matrix Inequalities [10]–[12], spectral conditions on Hamiltonian matrices [9], [13], and Frequency Domain Inequalities [2], [3]. The interested reader can refer to [14] for a review about the relationships between energetic characterizations of linear time invariant systems.

In this work, we consider general nonlinear circuit blocks (e.g. amplifiers and low-dropout voltage regulators) which are designed to operate under small-signal conditions, that is, all port signals exhibit small fluctuations around some constant bias levels. For such circuit blocks, it is a common practice to employ simplified linearized models in analysis and design flows. When such a linearization is associated with a simultaneous Model Order Reduction process [15], overall complexity and runtime in transient circuit simulation can be drastically reduced with respect to detailed transistor-level descriptions, in some cases by orders of magnitude [16]–[18].

Consider a general circuit block that does not include internal independent sources such as batteries, and interacts with the environment through well-defined electrical ports. When its behavior is analyzed at these ports, such circuit block is expected to be dissipative. Even if individual components such as for instance transistors and operational amplifiers are commonly denoted as *active*, they are in fact dissipative, and any arbitrary circuit block resulting from the interconnection of such components is also dissipative. However, when any of such systems is linearized around a reference operating point defined by externally applied bias/supply signals, the resulting small-signal model is in general not guaranteed to be dissipative, since it could potentially provide at its ports more power than it has been receiving and storing. The main objective of this work is to establish a generalization of the well-known dissipativity conditions, aimed at the precise characterization of the energy behavior of linearized models, so that the energy and power redistribution between bias and small signal components is mathematically evident.

In this paper, we will distinguish between *small-signal models*, whose inputs and outputs are small-signal variations around some operating point, and *linearized models*, whose inputs and outputs include also the (constant) bias or supply signals. Only linearized models can seamlessly replace the original circuit blocks in a circuit simulation environment, when the small-signal components of inputs and outputs are small. While small-signal models can be described in terms of regular linear state-space equations, linearized models require a slightly more general *affine* form (introduced in Sec. II), including a constant term in the output equation and thus taking into account both small variations and bias signals.

In this work, we focus on energy-preserving properties of such affine linearized models. We show that the well-known

T. Bradde, S. Grivet-Talocia, G.C. Calafiore, A.V. Proskurnikov are with the Dept. Electronics and Telecommunications, Politecnico di Torino, Torino 10129, Italy (e-mail: tommaso.bradde@polito.it, stefano.grivet@polito.it, giuseppe.calafiore@polito.it, anton.p.1982@ieee.org).

Z. Mahmood is with NanoSemi, Inc., Waltham, MA 02451, USA (e-mail: zohaib.mahmood@nanosemitech.com).

L. Daniel is with the Department of Electrical Engineering and Computer Science, Massachusetts Institute of Technology, Cambridge, MA 02139 USA (e-mail: luca@mit.edu).

dissipativity conditions for (homogeneous) linear state-space models are not applicable to such systems due to the presence of the constant bias/supply components. For this reason, we propose a generalization of these conditions,account for the fact that affine linearized models are meaningful only in the vicinity of a well-defined operating point, with the inputs restricted to a bounded set. We will in fact show that dissipativity of affine linearized models holds locally [19], but only if an explicit constraint on input boundedness is verified. We refer to this property as *Bounded-Input Dissipativity (BID)*. The proposed BID conditions provide a novel theoretical framework, which can be readily applied to enhance robustness in numerical circuit simulation. Specifically, BID conditions can be implemented as automated numerical checks to detect physically inconsistent behavior even during runtime. Examples include possibly diverging voltages and currents due to excess power generated by linearized circuit models operating outside their range of validity. The test cases of Sec. VII will demonstrate this concept.

Our approach is complementary to [20]–[23], where the local dissipativity properties of a nonlinear system are assessed through simpified models. Here the focus is on dissipativity of the simplified model itself, given an original dissipative large-scale nonlinear system. A similar problem is treated in the recent paper [24], which, however, confines the discussion to linear time invariant local models in standard form.

This paper is organized as follows. Sec. II introduces notation and some preliminaries and sets up the problem. Sec. III recalls basic definitions of dissipativity. In Sec. IV, we define BID conditions in integral and differential forms, which, as shown in Sec. V, can be reduced to convenient Bilinear Matrix Inequalities. In Sec. VI, we discuss several approaches for the verification of the proposed BID conditions with simultaneous maximization of the small-signal input amplitude for which the BID property is guaranteed. Several examples are used in Sec. VII to illustrate the above-mentioned concept and to validate the proposed theory and estimation algorithms.

II. Background and Problem Setting

A. Notation

We denote the δ-ball in $\mathbb{R}^M$ centered at 0 by

$$B_\delta = \{\tilde{u} \in \mathbb{R}^M : \|\tilde{u}\|_2 \leq \delta\}, \tag{1}$$

where $\delta \in \mathbb{R}$ a positive constant and $\|\cdot\|_2$ the standard Euclidean norm. The set of all one-sided signals whose amplitude is uniformly bounded by δ is denoted by

$$\mathcal{B}_\delta^0 = \{\tilde{u}(\cdot) : \tilde{u}(t) \in B_\delta \ \forall t \ \text{ and } \ \tilde{u}(t) \equiv 0 \ \forall t \leq 0\} \tag{2}$$

and the set of corresponding δ-bounded signals with a superimposed DC component U_0 is denoted by

$$\mathcal{B}_\delta^{U_0} = \{u(\cdot) : \ u(t) = U_0 + \tilde{u}(t) \ \ \forall t, \ \forall \tilde{u} \in \mathcal{B}_\delta^0\}. \tag{3}$$

For a symmetric matrix $W = W^\top$, we write $W \succ 0$ if W is positive definite (all its eigenvalues are positive).

B. Small-signal models

Our discussion starts from a generic nonlinear M-port system described in state-space form

$$\begin{aligned} \dot{\xi}(t) &= F(\xi(t), u(t)), \\ \eta(t) &= G(\xi(t), u(t)), \end{aligned} \tag{4}$$

where $u, \eta \in \mathbb{R}^M$ denote the input and output signals, $\xi, \dot{\xi} \in \mathbb{R}^N$ are the internal state vector and its time derivative, and F, G are C^1-smooth maps. Each port m defines two electrical variables (a voltage v_m and a current i_m), one corresponding to the m-th input $u_m(t)$ and the other corresponding to the m-th output $\eta_m(t)$. Therefore, only immittance (including impedance, admittance and hybrid) representations are considered. Henceforth all signals u, ξ, η are dimensionless, scaled by appropriate reference values $U_{\rm ref}, \Xi_{\rm ref}, Y_{\rm ref}$.

Next, we summarize the main steps that lead to a linearized system whose order n can be much smaller than the dimension of the original state N, and whose input-output properties approximate those of (4) in the vicinity of the operating point. We start by splitting all signals as

$$u(t) = U_0 + \tilde{u}(t), \quad \xi(t) = \Xi_0 + \tilde{\xi}(t), \quad \eta(t) = Y_0 + \tilde{\eta}(t), \tag{5}$$

with the following assumptions:

1) (U_0, Ξ_0, Y_0) is a well-defined asymptotically stable equilibrium point [25, Sec. 5], corresponding to the static input U_0 with (Ξ_0, Y_0) being the constant solution of (4)

$$\begin{aligned} 0 &= F(\Xi_0, U_0), \\ Y_0 &= G(\Xi_0, U_0) \end{aligned} \tag{6}$$

2) $\tilde{u}(t) \equiv 0$ for $t \leq 0$, and thus

$$u(t) = U_0, \quad \xi(t) = \Xi_0, \quad \eta(t) = Y_0, \quad \forall t \leq 0. \tag{7}$$

3) the small-signal condition in the input is imposed by constraining $\tilde{u} \in \mathcal{B}_\delta^0$ with a known bound $\delta > 0$.

These assumptions can be justified as follows. Conditions (6)-(7) coincide with the exact operations that are performed by any SPICE-like circuit solver for transient simulation. The operating point (6) is computed first, then transient time-stepping iterations are performed with initial conditions defined by the operating point (7). Furthermore, asymptotic stability of the operating point and small-signal operation are prerequisites for the correct functioning of the specific circuit blocks under investigation (e.g., linear amplifiers and low dropout voltage regulators). If these conditions are not met, using linearized small-signal models is inappropriate in the first place (this scenario is not of interest for this work).

Under assumptions 1)-3), an approximate small-signal model can be obtained by linearizing (4) around (Ξ_0, U_0)

$$\begin{aligned} \dot{\tilde{\xi}}(t) &\approx \tilde{A}\,\tilde{\xi}(t) + \tilde{B}\,\tilde{u}(t), \\ \tilde{\eta}(t) &\approx \tilde{C}\,\tilde{\xi}(t) + \tilde{D}\,\tilde{u}(t), \end{aligned} \tag{8}$$

where $\tilde{A}$, $\tilde{B}$, $\tilde{C}$, $\tilde{D}$ are the matrices of partial derivatives of maps F, G computed at the equilibrium (Ξ_0, U_0).

The dimension N of $\tilde{\xi}$ can be large, and Model Order Reduction techniques are often applied to reduce its complexity, leading to a generic *small-signal reduced-order model* of (4)

$$\begin{aligned} \dot{\tilde{x}}(t) &= A\,\tilde{x}(t) + B\,\tilde{u}(t), \quad \tilde{x}(0) = 0 \\ \tilde{y}(t) &= C\,\tilde{x}(t) + D\,\tilde{u}(t), \end{aligned} \tag{9}$$

with $\dim(\tilde{x}) = n \ll N = \dim(\tilde{\xi})$. The corresponding transfer function from $\tilde{u}$ to $\tilde{y}$ approximates the transfer function of (8)

$$\tilde{H}(s) = D + C(sI - A)^{-1}B \approx \tilde{D} + \tilde{C}(sI - \tilde{A})^{-1}\tilde{B} \tag{10}$$

up to an error that depends on the adopted reduction scheme. Classical projection [26] or truncation [27] methods or data-driven fitting approaches [28], [29] can be used for order reduction, for an overview, see [15]. All numerical examples in this paper result from application of the Vector Fitting algorithm [28] to a set of frequency response samples $\tilde{H}_k = \tilde{H}(j\omega_k)$ previously computed by a circuit solver at discrete frequencies ω_k. Henceforth we assume that the reduction process preserves asymptotic stability, so that all eigenvalues of A have a (strictly) negative real part.

C. Affine linearized models

We define the *affine linearized model* of (4) as a modification of the reduced-order model (9) as follows

$$\begin{aligned} \dot{x}(t) &= Ax(t) + Bu(t), \qquad x(0) = X_0 \\ y(t) &= Cx(t) + Du(t) + Y_C, \end{aligned} \tag{11}$$

where the constant vectors X_0, Y_C are defined as

$$Y_C = Y_0 - (CX_0 + DU_0) \quad \text{and} \quad X_0 = -A^{-1}BU_0. \tag{12}$$

Comparing (11) to (9), one notices that

1) model (11) is fed by the total input $u = U_0 + \tilde{u} \in \mathcal{B}_\delta^{U_0}$ rather than just its small-signal component $\tilde{u} \in \mathcal{B}_\delta^0$;
2) the output contains the constant term Y_C, which is needed to provide matching between (4) and (11) at the stationary regime $u(t) \equiv U_0$, $x(t) \equiv X_0 \implies y(t) \equiv Y_0$;
3) similarly to (5), we can split the signals $x(t)$ and $y(t)$ as

$$x(t) = X_0 + \tilde{x}(t), \quad y(t) = Y_0 + \tilde{y}(t), \tag{13}$$

where, due to the initial condition in (11), $\tilde{x}(t) = 0$ and $\tilde{y}(t) = 0$ for $t < 0$. In other words, the circuit is at rest for $t < 0$, where only the constant bias signals are applied.

The above conditions provide a consistent framework, where the original nonlinear circuit block can be replaced by its affine linearized model in a circuit simulation environment. Notice that there is no simple relation between the "genuine" equilibrium state Ξ_0 and X_0. Using (11) instead of (4), however, one has to define the initial condition X_0 as in (12) in order to guarantee that the constant components U_0 and Y_0, henceforth denoted as *DC components*, match exactly the input and output levels defining the operating point of (4). The signal $\tilde{y}(t) = y(t) - Y_0$ approximates the actual small-signal component $\tilde{\eta}(t)$ with an error introduced by the linearization and model reduction procedures. With reference to Fig. 1, which illustrates the above affine linearization process in the scalar (one-port) static case, we remark that both models (9) and (11) should be considered as valid approximations of (4) only if the deviations from the equilibrium point are sufficiently small. If this assumption is not verified, then different modeling strategies should be adopted, see e.g. [30].

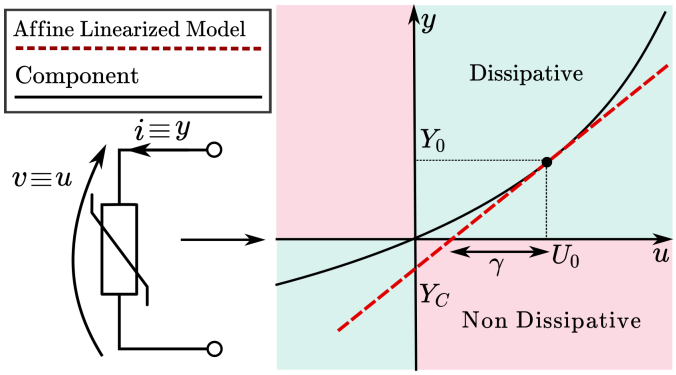

Fig. 1. The linearized affine model of a nonlinear dissipative static component in admittance representation. The presence of the biasing input U_0 allows to derive a local model around the operating point, corresponding to a constant output Y_0. The linearized model characteristic is affine, with a non-zero output Y_C obtained with a vanishing input voltage. An affine linearized model is meaningful only in the vicinity of the operating point. When the magnitude of the small-signal input $u - U_0$ exceeds γ, the linearized model may start to operate in the non-dissipative region.

D. Reachability sets of small-signal and affine linearized models

In order to study the local dissipativity properties of (11), we need a characterization of the set where its state can dwell when the input signal is bounded in amplitude. This reduces to analysis of the reachability set for the small-signal model (9) subjected to input $\tilde{u} \in \mathcal{B}_\gamma^0$, defined as follows.

Definition 1: The *reachability set* R_γ of (9) is the set of all states $\tilde{x}(t)$ that can be reached (in some finite time) from the initial state $\tilde{x}(0) = 0$ under some input $\tilde{u} \in \mathcal{B}_\gamma^0$, for given $\gamma \geq 0$. That is

$$R_\gamma = \{\tilde{x}(t) : t \geq 0 \text{ and (9) holds with } \tilde{u} \in \mathcal{B}_\gamma^0\}.$$

Due to the linearity, the states of the affine linearized model (11) reachable from $x(0) = X_0$ under inputs $u \in \mathcal{B}_\gamma^{U_0}$ constitute the set $X_0 + R_\gamma$, that is, the translation of the small-signal reachability set by the constant state bias X_0.

III. Background on Classical Dissipative Systems

Before introducing the BID conditions in Sec. IV, we recall some classical definitions and results on dissipative systems.

A. Classical dissipative systems

We start by recalling the well-known characterization of dissipative systems from [4], formulated in the considered immittance representation.

Definition 2: A system is *dissipative* if there exists a non-negative *storage function* of the state $E(x) \geq 0$ such that

$$E(x(t)) - E(x(0)) \leq \int_0^t u(\tau)^\top y(\tau)\, d\tau \quad \forall t \geq 0 \tag{14}$$

for any value of input vector u, output vector y and state vector x compliant with the system dynamics.

The storage function $E(x)$ can be interpreted as a level of *energy* stored in the system for a given value of the state vector x. The left-hand side of (14) represents the increase of such energy after t seconds of the system operation. For a dissipative system, such an increase cannot exceed the total energy received from the environment, expressed in the right as the time integral of the net input power flow (assumed positive when inward). We henceforth refer to the integral in (14) as the *cumulative energy flow*. If the function E is C^1-smooth, condition (14) can be cast in differential form as

$$\frac{d}{dt}E(x(t)) \leq u(t)^\top y(t) \quad \forall t \geq 0. \tag{15}$$

This last expression states that for a dissipative system the rate of change of the stored energy can not exceed the instantaneous power provided by the environment.

B. A particular case: the Kalman-Yakubovich-Popov Lemma for linear time-invariant systems

Consider the particular case of a linear and time-invariant system, such as (9). It is known [5, Theorem 3] that if a storage function satisfying the dissipation inequality (15) exists, it can be found within the class of positive definite quadratic forms: $E(x) = x^\top P x$ with $P \succ 0$. More formally, a *minimal* (controllable and observable) system (9) is dissipative if and only if the following Linear Matrix Inequality is feasible

$$\exists P \succ 0: \quad \tilde{z}^\top \Sigma_0(P)\, \tilde{z} \leq 0 \quad \forall \tilde{z} \tag{16}$$

where

$$\Sigma_0 = \begin{bmatrix} A^\top P + PA & PB - C^\top \\ B^\top P - C & -D - D^\top \end{bmatrix} \quad \text{and} \quad \tilde{z} = \begin{bmatrix} \tilde{x} \\ \tilde{u} \end{bmatrix}. \tag{17}$$

As discussed in [5], this statement is equivalent to the Kalman-Yakubovich-Popov lemma, and (16) is feasible if and only if the system satisfies the condition of positive realness.

IV. Bounded Input Dissipativity: BID

We now proceed to the main contribution of this work, namely the characterization of the energy properties of (11).

A. BID: integral form

Consider affine linearized system (11). In the adopted signal representation, both $u(t)$ and $y(t)$ include a DC and a small-signal component, so the input power flow can be written as

$$p(t) = u(t)^\top y(t) = (U_0 + \tilde{u}(t))^\top (Y_0 + \tilde{y}(t)). \tag{18}$$

Here the DC power component $P_0 = U_0^\top Y_0$ is fixed based on the operating point, and matches identically the DC power absorbed by the original system (4) in absence of small-signal components. A similar supply rate is used in [31] to characterize the so-called *Equilibrium Independent Passivity*.

The need for the concept of BID is clarified by the following example, which describes a practically relevant particular case.

Example 1: Let us assume that $P_0 > 0$. The sign of the small-signal power component $\tilde{p}(t) = \tilde{u}(t)^\top \tilde{y}(t)$ is unknown and can be even persistently negative $\forall t \geq 0$, which corresponds to a non-dissipative behavior of the small-signal model (consider an amplifier circuit as a typical example). Due to linearity, replacing $\tilde{u}$ with $a\tilde{u}$ causes $\tilde{p}$ to be rescaled by a^2. Then, there exists a critical value a_* for which the total power $p(t)$ becomes negative. We can thus expect that affine system (11) behaves as dissipative for small inputs $\tilde{u}$ and as non-dissipative when $\tilde{u}$ increases beyond a critical size.

The above qualitative considerations are now made more general and precise. We introduce the following definition.

Definition 3: The affine linearized system (11) is *Bounded Input Dissipative* (BID) with respect to the input amplitude level $\gamma \geq 0$ if there exists a continuous function $E(x)$ which satisfies (14) for any solution to (11) with input $u \in \mathcal{B}_\gamma^{U_0}$.

Remark 1: unlike the standard definition of dissipativity (Definition 2), we consider only solutions starting at the equilibrium point X_0, consistently with (11). Also, the assumption $E(x) \geq 0$ is dropped. If a continuous storage function satisfying (14) exists, one can always ensure that $E(x) \geq 0$ whenever $x(t) \in X_0 + R_\gamma$ by adding a sufficiently large positive constant $E(x) \leftarrow E(x) + c$. Provided that $u \in \mathcal{B}_\gamma^{U_0}$, the values $E(x)$ at the points $x \notin X_0 + R_\gamma$ play no role.

B. BID: differential form

Assuming that the storage function is smooth, we show that the integral inequality (14) is implied by the following algebraic inequality, which is similar to (15) and can be interpreted as the BID definition in differential form.

Lemma 1: Let $E(x)$ be a C^1-smooth function in some vicinity of $X_0 + R_\gamma$ satisfying the *dissipation inequality*

$$\frac{\partial E(x)}{\partial x}(Ax + Bu) \leq u^\top y, \tag{19}$$

for any vectors x, u, y such that $x - X_0 \in R_\gamma$, $u - U_0 \in B_\gamma$, $y = Cx + Du + Y_C$. Then any solution of (11) with $\tilde{u} \in \mathcal{B}_\gamma^0$ satisfies the integral inequality (14).

The proof of Lemma 1 is provided in Appendix A. Lemma 1 provides a purely algebraic sufficient condition for BID, entailing the following result to be proved in Appendix B.

Theorem 1: Consider a nonlinear system as in (4) and its affine linearization (11) corresponding to DC bias input U_0, state X_0, and output Y_0. If the system at the bias point is asymptotically stable and dissipates a strictly positive DC power $U_0^\top Y_0 > 0$, then there exists a non-zero $\gamma_* > 0$ such that the system is BID for any input $u \in \mathcal{B}_\gamma^{U_0}$ with $\gamma < \gamma_*$.

V. Verification of the BID property

The BID property may hold or fail depending on the amplitude γ of the small-signal input, e.g. Theorem 1 ensures this property for sufficiently small γ whenever $P_0 > 0$. Our aim in this section is to devise a numerically viable approach for checking whether system (11) is BID for a *given* input amplitude γ. Our approach will build on the algebraic condition provided by Lemma 1. At the second stage (Sec. VI), we will exploit this tool to estimate the maximum input amplitude $\gamma_{\max}$ for which BID is verified. The resulting bound $\gamma_{\max}$ will thus define a *trust region* for the small-signal inputs such that the energy behavior of the affine linearized model (11) is qualitatively consistent with the original system (4).

A. Overview

When the input of system (11) is bounded as $u \in \mathcal{B}_\gamma^{U_0}$, the corresponding state vector is confined to the reachability set $x \in X_0 + R_\gamma$. Therefore, verification of the BID property (19) for a given amplitude level γ requires the characterization of the reachability set R_γ defined in II-D, which is in general difficult to obtain in an exact form. Therefore, we will resort to an approximate characterization based on overbounding R_γ by an ellipsoid (Sec. V-C). This will produce an algebraic condition for BID (Sec. V-D) which can be easily tested in finite time, once a suitable parameterization of the storage function E in a sufficiently large class is devised (Sec. V-B).

We remark that our requirements are very different from common scenarios in the control literature, where the original system is a plant, whose behavior is to be made compliant with given performance criteria via control design. Sometimes these criteria are even based on full state constraints, as in the recent works [32], [33]. Here, the states have no particular physical meaning, being the result of a black-box input-output reduced-order identification; therefore, state constraints in any form, including approximate estimation through dedicated observers [34], loose practical significance. Hence, we do not enforce any constraints on the system, but rather wish to check, possibly in runtime during circuit simulation, whether the reduced-order linearized model has an energy behavior that is consistent with the original nonlinear circuit block.

B. Storage functions

As discussed in Sec. III-B, dissipativity of a LTI state-space system implies the existence of a storage function in the class of positive definite quadratic forms in view of the Kalman-Yakubovich-Popov lemma. The BID property instead admits more general storage functions, in particular, the condition of positivity can be discarded. One open problem is to determine a "minimal" class of potential storage functions with a suitable parametrization to be used for numerical BID verification.

In order to address this issue, this paper derives sufficient criteria for BID by employing quadratic storage functions

$$E(x) = \frac{1}{2} x^\top P x + q^\top x \tag{20}$$

where $P = P^\top$ is a symmetric matrix (possibly, with negative eigenvalues), and q is a vector. This class of functions will still allow us to derive efficient criteria for BID, that work in many practically important cases. Notice that the presence of a linear term in (20) is important and may visibly increase the numerically-determined small-signal input amplitude for which the BID property can be established, see Sec. VII.

C. Approximation of the Reachability Set

The reachability set R_γ discussed in Sec. II-D is a closed and bounded set that includes the origin. Therefore, it is possible to embed and overbound R_γ by an ellipsoid $\mathcal{E}_{W,\gamma} \doteq \{\tilde{x} : \tilde{x}^\top W \tilde{x} \leq \gamma^2\}$ parameterized via an appropriate matrix $W \succ 0$. The following lemma allows us to find such an ellipsoid by solving a feasibility problem involving a specific Bilinear Matrix Inequality.

Lemma 2: Given an input amplitude bound $\gamma > 0$, if there exists a matrix $W \succ 0$ and a scalar $\alpha_r \geq 0$ satisfying the matrix inequality

$$\begin{bmatrix} A^\top W + W A + \alpha_r W & W B \\ B^\top W & -\alpha_r I \end{bmatrix} \preceq 0, \tag{21}$$

then $R_\gamma \subseteq \mathcal{E}_{W,\gamma} \doteq \{\tilde{x} : \tilde{x}^\top W \tilde{x} \leq \gamma^2\}$.

The proof of Lemma 2 for input amplitude bound $\gamma = 1$ is given in [35]. The extension to general $\gamma > 0$ is immediate since due to the linearity of (9) the reachable set for $\gamma > 0$ is a γ-inflated version of R_1, i.e., $R_\gamma = \gamma R_1$. Therefore, $R_1 \subseteq \mathcal{E}_{W,1}$ is equivalent to $R_\gamma \subseteq \gamma \mathcal{E}_{W,1} = \mathcal{E}_{W,\gamma}$.

D. Algebraic conditions for Bounded Input Dissipativity

We are now going to provide a sufficient condition for bounded input dissipativity.

Theorem 2: If for some $\gamma > 0$ the following inequality holds

$$\begin{aligned} &\tilde{z}^\top \Sigma_0(P) \tilde{z} + 2\theta_0(P,q)^\top \tilde{z} + \phi_0 \leq 0, \\ &\forall \tilde{x}, \tilde{u} : \quad \tilde{x}^\top W \tilde{x} \leq \gamma^2, \, \tilde{u}^\top \tilde{u} \leq \gamma^2 \end{aligned} \tag{22}$$

where $\Sigma_0(P)$ and $\tilde{z}$ are defined in (17),

$$\begin{aligned} \theta_0 &= \begin{bmatrix} A^\top (P X_0 + q) - C^\top U_0 \\ B^\top (P X_0 + q) - D^\top U_0 - Y_0 \end{bmatrix}, \\ \phi_0 &= -2 U_0^\top Y_0, \end{aligned} \tag{23}$$

and matrix W satisfies the conditions of Lemma 2, then affine linearized system (11) is BID with input amplitude level γ.

Proof: Condition (22) can be obtained by substituting the quadratic storage function (20) into the differential BID dissipation inequality (19) together with the assumptions of Lemma 1, and using the state space equations (11) to simplify the resulting expression. Clearly, if (22) holds, then (19) is verified and the system (11) is BID for the given input amplitude level γ. ∎

Note that (22) is only a sufficient condition for BID, due to the overbounding approximation of the actual reachable set.

The BID condition (22) to be verified differs from the standard condition (16) employed by the Kalman-Yakubovich-Popov lemma. First, inequality (22) includes some additional terms with a direct physical interpretation. The constant factor ϕ_0 represents the DC power contribution, whereas the linear factor represents the cross-coupling between DC (the various terms in vector θ_0) and small-signal power flows. This factor provides a precise characterization of the stored energy and power redistribution between signal components. Second, whereas (16) does not constrain the stack vector $\tilde{z}$, the BID condition (22) should hold under two additional constraints on its components. If these constraints are removed ($\gamma = \infty$, that is, the input is unconstrained), all DC components are set to zero, and the storage function is a positive definite quadratic form, then (22) reduces to condition (16).

A direct numerical verification of condition (22) is problematic due to the quadratic constraints on $\tilde{u}$ and $\tilde{x}$. A simpler condition can however be obtained by applying the so-called $\mathcal{S}$-procedure [36], which gets rid of the constraints on $\tilde{x}, \tilde{u}$ by introducing two auxiliary variables.

Lemma 3: Given the affine linear system (11) with input amplitude γ, condition (22) is implied by the existence of two constants $\alpha_x, \alpha_u \geq 0$ such that

$$\tilde{z}^\top \Sigma(P, W, \alpha_x, \alpha_u)\tilde{z} + 2\theta(P,q)^\top \tilde{z} + \phi \leq 0 \quad \forall \tilde{z}, \tag{24}$$

where Σ, θ, ϕ are defined as follows

$$\Sigma = \begin{bmatrix} A^\top P + PA - \alpha_x W & PB - C^\top \\ B^\top P - C & -D - D^\top - \alpha_u I \end{bmatrix}, \quad \theta = \theta_0 \qquad \phi = (\alpha_x + \alpha_u)\gamma^2 + \phi_0. \tag{25}$$

The inequality (24), obtained by applying again the $\mathcal{S}$-procedure to the inequalities (22), presents the advantage of having no explicit constraints in $\tilde{z}$ and can therefore be cast as the equivalent Bilinear Matrix Inequality condition

$$\begin{bmatrix} \Sigma(P, W, \alpha_x, \alpha_u) & \theta(P,q) \\ \theta(P,q)^\top & \phi(\alpha_x, \alpha_u, \gamma) \end{bmatrix} \preceq 0. \tag{26}$$

Recalling now that matrix W has to satisfy the inequality (21), we are now ready to formulate our main result. The following theorem provides an algebraic BID condition.

Theorem 3: Suppose that there exist matrices $W \succ 0$, $P = P^\top$, a vector q and scalars $\alpha_r, \alpha_x, \alpha_u \geq 0$ such that

$$\begin{bmatrix} A^\top W + WA + \alpha_r W & WB \\ B^\top W & -\alpha_r I \end{bmatrix} \preceq 0 \tag{27}$$

$$\begin{bmatrix} \Sigma(P, W, \alpha_x, \alpha_u) & \theta(P,q) \\ \theta(P,q)^\top & \phi(\alpha_x, \alpha_u, \gamma) \end{bmatrix} \preceq 0, \tag{28}$$

with Σ, θ, ϕ defined in (25). Then the system (11) is BID with the storage function (20) and the input amplitude level γ.

Proof: The inequality (28) is equivalent to (24), which by Lemma 3 implies (22). Since W and α_r satisfy (27), Lemma 2 guarantees that the ellipsoid $\tilde{x}^\top W \tilde{x} \leq \gamma^2$ contains all states reachable via inputs $\tilde{u} \in \mathcal{B}_\gamma^0$. Theorem 2 thus implies that system (11) is BID with respect to input amplitude γ. ■

The inequalities in (28) are bilinear since Σ involves the term $\alpha_x W$, ϕ involves the term $(\alpha_x + \alpha_u)\gamma^2$ and (27) involves the term $\alpha_r W$. However, for fixed $\alpha_x, \alpha_r, \alpha_u$ they reduce to usual LMIs with unknowns W, P, q and γ^2.

VI. Maximizing the input amplitude

The BID definition assumes that the small-signal input $\tilde{u}(t)$ belongs to a ball of radius γ, the latter entering the definition as a parameter. Clearly, if a system is BID for a given γ, it is also BID for any γ_1 such that $0 < \gamma_1 < \gamma$. Therefore, our objective will be in the following to identify the largest $\gamma_{\max}$ for which the inequalities (28) are feasible. We propose three different approaches to solve this optimization problem.

1) Direct check of Bilinear Matrix Inequality feasibility: The simplest and most direct approach is to check the feasibility of matrix inequalities (27)-(28). With this strategy, the maximum allowed input amplitude is found by sweeping the variable γ and checking for each value the feasibility of the conditions involved in Theorem 3. It is known that checking the feasibility of a Bilinear Matrix Inequality is a non-convex problem; nevertheless, commercial solvers are available which are able to tackle this problem. For this study, the solver *Penlab* [37] was exploited. We will show in Sec. VII that this direct approach may fail in some cases due to the solver's pecularities, so we present two alternative approaches, which are summarized below as Algorithms 1 and 2.

2) Alternate-coordinate optimization: The conditions of Theorem 3 are bilinear, however, once the scalar coefficients $\{\alpha_r, \alpha_u, \alpha_x\}$ are fixed, these conditions are linear in the remaining variables. Hence, an estimate of the maximum γ for which BID holds can be found through an alternate-coordinate optimization procedure, iterating two successive steps.We start with initializing $\{\alpha_{r*}, \alpha_{u*}, \alpha_{x*}\}$ to some suitable values.

At step 1, we solve the following semidefinite program:

$$\begin{aligned} &\underset{P,q,W,\gamma}{\text{maximize}} \quad \gamma \\ &\text{subject to} \\ &\begin{bmatrix} A^\top W + WA + \alpha_{r*} W & WB \\ B^\top W & -\alpha_{r*} I \end{bmatrix} \preceq 0 \\ &\begin{bmatrix} \Sigma(P, W, \alpha_{x*}, \alpha_{u*}) & \theta(P,q) \\ \theta(P,q)^\top & \phi(\alpha_{x*}, \alpha_{u*}, \gamma) \end{bmatrix} \preceq 0 \\ &W \succ 0 \\ &P = P^\top \end{aligned} \tag{29}$$

where $\{\alpha_{r*}, \alpha_{u*}, \alpha_{x*}\}$ are fixed. Once the local maximizers of (29) P_*, W_*, q_* and γ_* are obtained, at step 2 another Semidefinite Programming Problem is to be solved:

$$\begin{aligned} &\underset{\alpha_x, \alpha_u, \alpha_r, q, P}{\text{minimize}} \quad \alpha_x + \alpha_u \\ &\text{subject to} \\ &\begin{bmatrix} A^\top W_* + W_* A + \alpha_r W_* & W_* B \\ B^\top W_* & -\alpha_r I \end{bmatrix} \preceq 0 \\ &\begin{bmatrix} \Sigma(P, W_*, \alpha_x, \alpha_u) & \theta(P,q) \\ \theta(P,q)^\top & \phi(\alpha_x, \alpha_u, \gamma_*) \end{bmatrix} \preceq 0 \\ &\alpha_x \geq 0, \quad \alpha_u \geq 0, \quad \alpha_r \geq 0, \quad P = P^\top. \end{aligned} \tag{30}$$

where the scalar coefficients α_x, α_u, α_r, and q, P are considered as variables, while W_* and γ_* are held fixed. The minimizers of (30), α_{x*}, α_{u*} and α_{r*} can next be used as fixed parameters in (29), and the process is repeated.

The iteration of these two optimization steps allows one to obtain the desired estimate of $\gamma_{\max}$ for which BID holds. The heuristic choice of the cost function $\alpha_x + \alpha_u$ at step 2 is motivated by the structure of $\phi(\alpha_x, \alpha_u, \gamma)$ in (25): the reduction of $\alpha_x + \alpha_u$ may lead to increase in γ. We further impose the sequence of γ_* values generated by the algorithm to be nondecreasing and stop the iteration as soon as we detect that γ_* has decreased with respect to the previous iteration.

From a theoretical point of view, the approach is a heuristic non-convex optimization method, which is not guaranteed to converge to the global optimum. The non-decreasing sequence γ_* converges to a limit, being its supremum value and giving a lower estimate for the optimal value of γ. At the same time, in our experiments we observed rapid convergence, in a few iterations, to good locally optimal points.

3) Decoupling of the Bilinear Matrix Inequality: This approach is based on decoupling the two conditions (27)-(28) and works in two successive steps. First, an approximation of the reachability set R_γ is obtained by finding a matrix W of

maximum trace and a scalar α_r satisfying (27), solving the following optimization problem

$$\begin{aligned} \underset{W,\alpha_r}{\text{maximize}} \quad & \text{Trace}(W) \\ \text{subject to} \quad & \left[\begin{array}{cc} A^\top W + WA + \alpha_r W & WB \\ B^\top W & -\alpha_r I \end{array} \right] \preceq 0 \\ & \alpha_r \geq 0 \\ & W \succ 0 \end{aligned} \tag{31}$$

The maximal trace corresponds to the minimal "size" of the ellipsoid, understood as the sum of its squared semi-axes, and leads to the "tightest" approximation of the reachability set. The maximization can be achieved either by solving the bilinear problem or by sweeping on the variable α_r and solving the resulting linear matrix inequality. This first step provides a matrix W_*, which is substituted into (28) as a fixed parameter. For a fixed γ, the resulting inequality is also linear. Hence, we can find the maximum γ through a one-dimensional search by iteratively checking the feasibility of

$$\begin{aligned} & \exists P = P^\top, q, \alpha_x \geq 0, \alpha_u \geq 0 : \\ & \left[\begin{array}{cc} \Sigma(P, W_*, \alpha_x, \alpha_u) & \theta(P,q) \\ \theta(P,q)^\top & \phi(\alpha_x, \alpha_u, \gamma) \end{array} \right] \preceq 0. \end{aligned} \tag{32}$$

The decoupling algorithm also may fail to find the largest amplitude level γ, since in the statement of Theorem 3 the two constraints are actually coupled through the matrix variable W. Numerical experiments show that approaches 2) and 3) return same numerical results for all investigated test cases, however, approach 2) requires less computational time.

Algorithm 1 Alternate-coordinate optimization

Input: Linearized model parameters A, B, C, D, U_0, Y_0
Input: stop tolerance ϵ, maximum iterations K
Output: Estimated maximum input amplitude $\gamma_{\max}$

Set $\gamma^0_{\max} \leftarrow 0$, $k \leftarrow 1$
Find initial α_{r*}, α_{u*}, α_{x*} for which (29) is feasible
while $k \leq K$ **do**
  $\alpha_r \leftarrow \alpha_{r*} \quad \alpha_u \leftarrow \alpha_{u*} \quad \alpha_x \leftarrow \alpha_{x*}$
  Solve problem (29) for maximizers P_*, W_*, γ_*, q_*
    $W \leftarrow W_*, \quad \gamma \leftarrow \gamma_*, \quad \gamma^k_{\max} \leftarrow \gamma_*$
  if $|\gamma^k_{\max} - \gamma^{k-1}_{\max}| \leq \epsilon$ **then**
    $\gamma_{\max} \leftarrow \gamma^k_{\max}$
    break
  else if $\gamma^k_{\max} \leq \gamma^{k-1}_{\max}$ **then**
    $\gamma_{\max} \leftarrow \gamma^{k-1}_{\max}$
    break
  end if
  Solve problem (30) for minimizers α_{x*}, α_{u*}, α_{r*}
  $k \leftarrow k + 1$
end while
return: $\gamma_{\max}$

VII. Experimental Results

A. General considerations

The numerical assessment of the BID property will be performed by studying five different linearized models. For each of them, we will perform two types of experiments. At first, we will apply the methods exposed in Sec. VI in order to find the maximum amplitude level $\gamma_{\max}$ ensuring BID; we also show that the choice of purely quadratic candidate storage functions provides more restrictive (conservative) estimates of $\gamma_{\max}$ with respect to the adopted more general form (20).

Algorithm 2 Decoupling of the Bilinear Matrix Inequalities

Input: Linearized model parameters A, B, C, D, U_0, Y_0
Input: Search bound α_r^M, step sizes Δ_α, Δ_γ
Output: Estimated maximum input amplitude $\gamma_{\max}$

Set $\gamma \leftarrow 0$, $k^M \leftarrow \lfloor \alpha_r^M / \Delta_\alpha \rfloor$
for $k = 0, 1, \ldots, k^M$ **do**
  Set $\alpha_r \leftarrow k\Delta_\alpha$
  Find W_k that solves (31) with fixed α_r
end for
Find k_* for which $\text{Trace}(W_k)$ is maximum and set $W_* \leftarrow W_{k_*}$
while (32) is feasible with fixed γ **do**
  $\gamma \leftarrow \gamma + \Delta_\gamma$
end while
$\gamma_{\max} \leftarrow \gamma$

Since Theorem 3 provides only a sufficient BID condition, a second empirical verification strategy will be aimed at estimating the degree of conservatism of the computed input bound $\gamma_{\max}$. This task will be accomplished by running a set of transient analyses aimed at evaluating the behavior of the cumulative energy flow (the integral in (14), i.e., the total energy received by the system from the environment), by increasing the amplitude of a specifically designed small-signal test input. In fact, the divergence of this integral to $-\infty$ for a given input amplitude level γ provides an empirical proof that the system is not behaving as dissipative, since no storage function obeying (14) can exist under this condition. For this experimental evaluation we will confine ourselves to periodic small-signal inputs, which allow to certify the lack of dissipativity by means of finite-time transient simulations.

1) Designing test signals: We design test signals as follows. Denoting with $H(\jmath\omega)$ the frequency response of the trasfer matrix associated with matrices A, B, C, D in (11), we consider its Hermitian part $Q(\jmath\omega) = (H(\jmath\omega) + H(\jmath\omega)^{\mathsf{H}})$, noting that the quadratic form associated to $Q(\jmath\omega)$ corresponds up to a scaling constant to the active power absorbed by the system under sinusoidal steady-state conditions at frequency ω. Based on the eigenvector decomposition

$$Q(\jmath\omega)\mu_m(\jmath\omega) = \lambda_m(\jmath\omega)\mu_m(\jmath\omega) \tag{33}$$

we find the smallest eigenvalue

$$\lambda_* = \arg\min_{\omega,m} \lambda_m(\jmath\omega) \tag{34}$$

with associated eigenvector as μ_* and frequency of occurrence ω_*. A sinusoidal excitation at frequency ω_* with phasor input defined by the mode μ_* will thus lead to a power flow into the device equal to λ_*. If $\lambda_* < 0$, then the system is physically supplying power to its environment.

Based on the above considerations, we define each component of a sinusoidal small-signal test input as

$$\bar{u}_1^i(t) = |\mu_*^i| \cos(\omega_* t + \angle\mu_*^i) \quad \forall t > 0 \tag{35}$$

where μ_*^i is the i-th component of μ_*. In our numerical experiments, we have found that a square wave with the same amplitude/phase configuration defined as

$$\bar{u}_2^i(t) = |\mu_*^i| \text{sgn}(\cos(\omega_* t + \angle\mu_*^i)) \quad \forall t > 0 \tag{36}$$

leads to a less conservative estimation of the BID input bound, therefore the latter will be used in all numerical tests. The actual test signals used for testing a given bound γ are then

$$\tilde{u}_{1,2}(t) = \gamma \frac{\bar{u}_{1,2}(t)}{\max_t \|\bar{u}_{1,2}(t)\|_2}. \quad (37)$$

The critical value of γ for which the cumulative energy flow becomes persistently negative will be denoted throughout this section as γ_{exp}. As a result, we can guarantee that

- for $\gamma < \gamma_{\max}$ computed as in Sec. VI the system behaves as BID;
- for $\gamma \geq \gamma_{\text{exp}}$ the system is guaranteed not to be BID compliant, since a test input signal is found for which the inequality (14) fails to hold.

Therefore, the maximum allowed input amplitude γ_* is within the range $[\gamma_{\max}, \gamma_{\text{exp}})$. The degree of conservatism of the proposed approach can thus be estimated as $\beta = \gamma_{\max}/\gamma_{\text{exp}}$.

2) A particular case: There is a particular case for which the input amplitude γ_{exp} of signals $\tilde{u}_1(t)$ and $\tilde{u}_2(t)$ for which the system switches from BID to non-BID can be found analytically, providing also a quantitative explanation of why $\tilde{u}_2(t)$ is more suitable than $\tilde{u}_1(t)$ for our tests. Consider a 2-port system in form (11) for which the minimum eigenvalue λ_* occurs at frequency $\omega_* = \infty$, with a corresponding eigenvector $\mu_* = (1, 0)^\top$. Suppose in addition that the state space matrix D is symmetric. The test signal (35) and the corresponding small-signal output reduce to

$$\tilde{u}_1(t) = \gamma \begin{bmatrix} \cos(\omega_* t) \\ 0 \end{bmatrix}, \quad \tilde{y}_1(t) = D\tilde{u}_1(t) = \frac{\lambda_*}{2}\tilde{u}_1(t) \quad (38)$$

Assuming steady-state operation, the integral (14) does not diverge to $-\infty$ if and only if the active power absorbed by the circuit over one period is positive. Since

$$\begin{aligned} p(t) &= (\tilde{u}(t) + U_0)^\top (\tilde{y}(t) + Y_0) = \\ &= \gamma^2 \frac{\lambda_*}{2} \cos(\omega_* t)^2 + \gamma \cos(\omega_* t) Y_0^1 + \\ &+ \gamma \frac{\lambda_*}{2} U_0^1 \cos(\omega_* t) + {U_0}^\top Y_0 \end{aligned} \quad (39)$$

we find the maximum value of γ for which the average power over one period is nonnegative as

$$\int_0^{\frac{2\pi}{\omega_*}} p(t)dt \geq 0 \quad (40)$$

which leads to the bound

$$\gamma_1 \leq \gamma_{\text{exp},1} = \sqrt{\frac{4{U_0}^\top Y_0}{|\lambda_*|}}. \quad (41)$$

The same derivation can be carried out for the square wave test signal (36)

$$\tilde{u}_2(t) = \gamma \begin{bmatrix} \text{sgn}(\cos(\omega_* t)) \\ 0 \end{bmatrix} \quad (42)$$

which leads to the following bound

$$\gamma_2 \leq \gamma_{\text{exp},2} = \sqrt{\frac{2{U_0}^\top Y_0}{|\lambda_*|}} < \gamma_{\text{exp},1}. \quad (43)$$

Therefore, the square wave (in this special case) gives a less conservative estimate of the upper bound for γ.

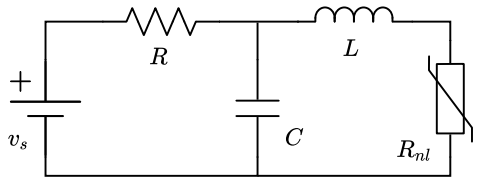

Fig. 2. A second-order circuit including a nonlinear resistor.

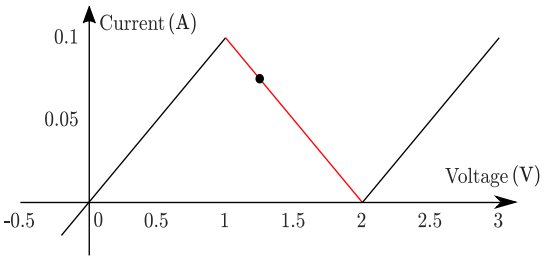

Fig. 3. Non-linear resistor characteristic and operating point (dot).

B. A minimal complexity illustrative example

We first illustrate the proposed methods by analyzing the BID property of the minimal circuit, shown in Fig. 2. The circuit parameters are $v_s(t) = V_{dd} + \tilde{v}(t)$ with $V_{dd} = 8.75\,\text{V}$, $R = 100\,\Omega$, $C = 80\mu\text{F}$, $L = 0.1\,\text{H}$, and where R_{nl} is a non-linear resistor with $V - I$ characteristic shown in Fig. 3.

We are interested in the behavior of the one-port element connected to the voltage source v_s in the admittance representation, assuming the voltage source as input and the corresponding current as output. The biasing current I_0 is equal to 0.075A and represents the DC output of our circuit.

A small signal equivalent circuit valid in the vicinity of the operation point can be obtained by replacing the non-linear element with its Thevenin equivalent, with a (negative) differential resistance $R_d = -10\Omega$ and an offset voltage generator $V_{0nl} = 2\text{V}$. The resulting linear circuit admits the second-order state-space representation (11), where according to our notation we have $U_0 = V_{dd}$, $Y_0 = I_0$ and $\tilde{u}(t) = \tilde{v}(t)$. The small signal output $\tilde{y}(t)$ coincides with the approximated

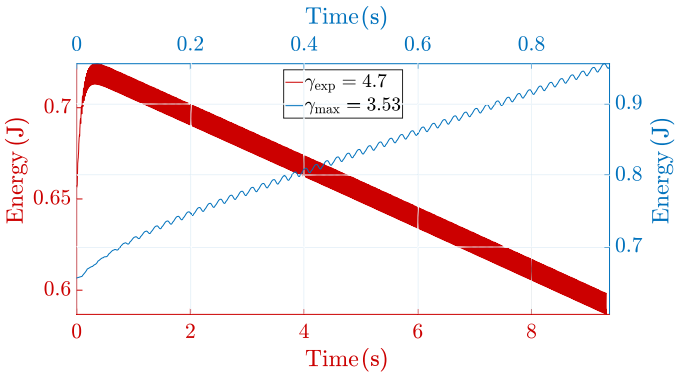

Fig. 4. Cumulative energy flow under square wave excitation of the second order circuit example for two different input amplitudes. For input amplitude $\gamma_{\text{exp}} = 4.7$, the cumulative energy entering the model diverges to an arbitrarily large negative amount (time scale is extended to show this behavior). Therefore, no storage function satisfying (14) exists and thus the system is not BID if the amplitude level reaches γ_{exp}.

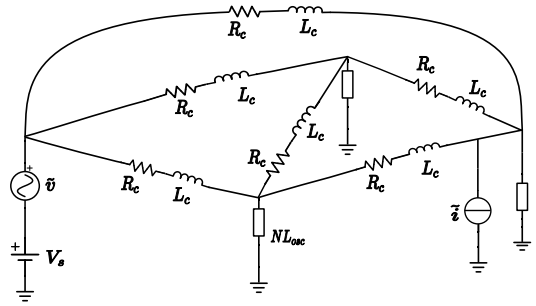

Fig. 5. Structure of a network of coupled nonlinear oscillators.

small signal response $\tilde{i}(t)$ of the linearized circuit.

The three optimization procedures presented in Sec. VI are then applied to the resulting system to estimate the maximum amplitude $\gamma_{\max}$ that $\tilde{v}$ can attain in order to preserve the BID condition. All three methods return the same result $\gamma_{\max} = 3.53\,\mathrm{V}$. Repeating the experiments by confining the research of purely quadratic storage functions, the bound reduces to $\gamma_{\max}|_{q=0} = 1.66$ V and $\gamma_{\max}|_{q=0} = 0.64$ V for methods 1,3 and 2, respectively. These results confirm that purely quadratic storage functions are not general enough for BID verification, since the set of allowed input signal is in fact larger when using the proposed more general form (20).

At the second stage, the linearized model was simulated making use of a small signal $\tilde{u}_2$ with amplitude $\gamma = \gamma_{\max}$, and the cumulative energy flow was evaluated numerically. The top panel of Fig. 4 confirms that this energy flow is always positive: the system is continuously absorbing energy in agreement with the physical condition for dissipativity. We now increase the input amplitude until we experimentally verify that the trend of the energy flow changes sign, as depicted in the bottom panel of Fig. 4. The dissipation inequality holds until the amplitude $\gamma_{\exp} = 4.7$ V is reached. Beyond this level, the cumulative energy flow not only becomes negative at a given time horizon, but in fact linearly decreases to $-\infty$. The exact input amplitude bound γ_* for which BID holds is in the range $[\gamma_{\max}, \gamma_{\exp})$, with $\beta = 0.75$.

C. A network of coupled oscillators

The second test case is a network of coupled oscillators (Fig. 5). The main building block is a nonlinear LC oscillator (Fig. 6), where the nonlinear resistor has a non-monotonic piecewise-linear current-controlled characteristic shown in Fig. 7. All oscillator cells are connected by RL branches, with a single node connected to a voltage source $v_s(t) = V_s + \tilde{v}_s(t)$. A small-signal current source $\tilde{i}_d(t)$ is connected in parallel to one of the oscillators. Excluding the sources, a two-port system is obtained, which is described in hybrid representation.

The above general structure was tested in many different configurations, by parameterizing number of nodes, connectivity of the coupling network, and component values. We report the results of a 13-cell structure with a fully connected ($R_C = 14.5\,\Omega$, $L_C = 0.15$ mH) coupling network. Each oscillator cell has a fixed resistance $R = 0.5\Omega$ and a resonance

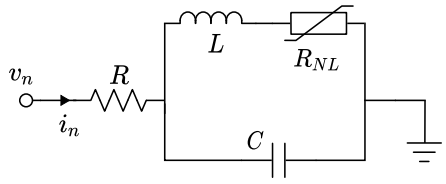

Fig. 6. A single oscillator cell forming the network of Fig. 5.

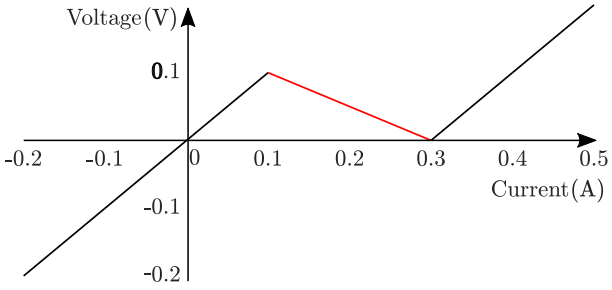

Fig. 7. Characteristic of the non-linear resistor in the oscillator cells. Each coupled oscillator is biased with operating point belonging to the red segment.

frequency $\frac{1}{\sqrt{LC}}$ which ranges from $\omega_{\min} = 200$ rad/s to $\omega_{\max} = 283$ rad/s. The bias voltage is $V_s = 2$ V.

For the particular network realization that we report here, we have a DC solution (with small-signals switched off)

$$U_0 = \begin{bmatrix} V_s \\ I_d \end{bmatrix} = \begin{bmatrix} 2\,\mathrm{V} \\ 0\,\mathrm{A} \end{bmatrix} \qquad Y_0 = \begin{bmatrix} I_s \\ V_d \end{bmatrix} = \begin{bmatrix} 1.66\,\mathrm{A} \\ 0.15\,\mathrm{V} \end{bmatrix}. \quad (44)$$

The particular combination of the network parameters was determined by trial and error, such that the nonlinear resistor of each oscillator is biased in the active region, displayed in red in Fig. 7.

The linearized equivalent is cast in form (11) and has dimension $N = 117$. The eigenvalues of the system matrix A have a strictly negative real part. The system is thus asymptotically stable in the vicinity of the operation point, but the resulting small-signal linearization behaves as locally active. As a confirmation, Fig. 8 reports one of the frequency-dependent Hermitian eigenvalues $\lambda(\jmath\omega)$ of the small-signal transfer matrix $H(\jmath\omega)$, which attains negative values in a well-defined frequency band. In order to reduce complexity, the system was subjected to model order reduction, reducing the dimension to $n = 20$. Figure 9 shows that no significant accuracy loss arises from the model order reduction process.

The two methods of Sec. VI-2 and VI-3 lead to the same estimate $\gamma_{\max} = 0.43$ in 5 s and 75 s, respectively. Restricting the storage function to a quadratic form returned instead $\gamma_{\max}|_{q=0} = 0.36$ with method 3, while method 2 is early stopped after the first iteration due to a non-increasing estimate of γ. Similarly to the previous test case, the transient simulation of the linearized system leads to a larger input bound $\gamma_{\exp} = 0.53$, so that we infer that $\gamma_* \in [0.43, 0.53)$, with $\beta = 0.81$. The corresponding cumulative energy flow (diverging to $-\infty$) resulting from the test signal (36) with amplitude $\gamma_{\exp}$ is shown in Fig. 10, confirming that the linearized model behaves as non-dissipative for $\gamma = \gamma_{\exp}$.

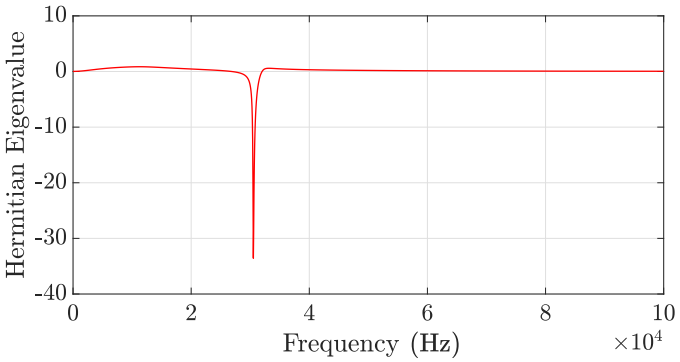

Fig. 8. Frequency-dependent trajectory of one eigenvalue of $Q(\jmath\omega) = (H(\jmath\omega) + H(\jmath\omega)^{\mathsf{H}})$ of the coupled oscillator network.

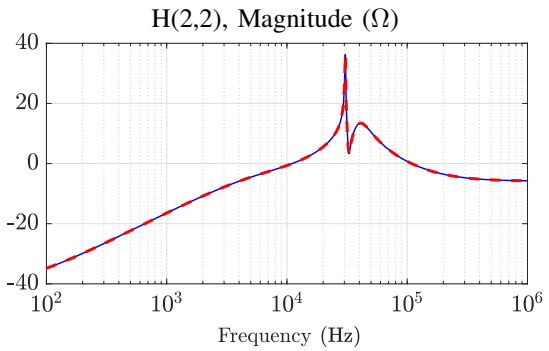

Fig. 9. Coupled oscillator network: frequency responses of selected elements of the trasfer matrix. Blue: original system; red: reduced order model.

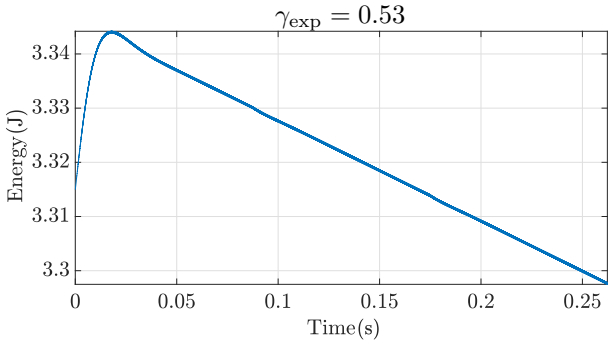

Fig. 10. Cumulative energy flow (as in Fig. 4) for the coupled oscillators network.

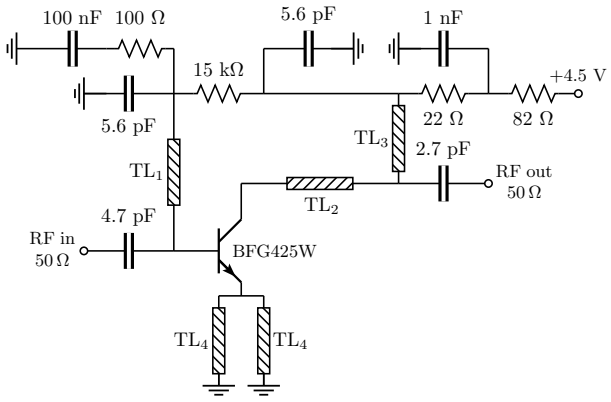

Fig. 11. A Low Noise Amplifier circuit [38].

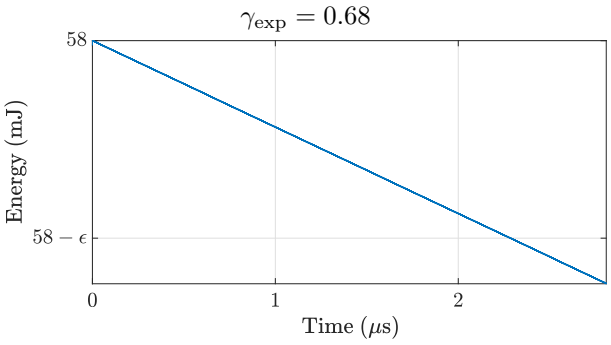

Fig. 12. Cumulative energy flow (as in Fig. 4) for the low noise amplifier test case.

D. An Low Noise Amplifier circuit

We now consider a Low Noise Amplifier circuit for radio-frequency operation working at 2 GHz, depicted in Fig. 11. See [38] for additional details. Considering an admittance representation, the DC supply/bias levels are

$$U_0 = \begin{bmatrix} V_{\text{in}} \\ V_{\text{out}} \\ V_{\text{sup}} \end{bmatrix} = \begin{bmatrix} 0 \\ 0 \\ 4.5 \end{bmatrix} \text{V}, \quad Y_0 = \begin{bmatrix} I_{\text{in}} \\ I_{\text{out}} \\ I_{\text{sup}} \end{bmatrix} = \begin{bmatrix} 0 \\ 0 \\ 13 \end{bmatrix} \text{mA}$$

Due to the presence of the lossy transmission line segments, characterized by frequency-domain telegrapher's equations with frequency-dependent parameters to represent skin and dielectric losses, it is not possible to cast the system dynamics as a finite-dinemsional state-space form. Therefore, we identify a local linearized equivalent by means of the Vector Fitting algorithm [28], applied to frequency samples obtained by a small-signal frequency response sweep. The result is an affine state-space form (11) with $n = 30$ states.

For this case study, application of the direct Bilinear Matrix Inequality feasibility check of Sec. VI-1 turned out to be impractical, since the verification of the feasibility of conditions (27) (28) for a single fixed γ required more than one hour. Conversely, the other two methods of Sec. VI-2 and Sec. VI-3 returned the same solution $\gamma_{\max} \approx 0.58$ V in approximately 8 s and 64 s, respectively. Unlike the example of Sec. VII-B, the usage of purely quadratic storage functions ($q = 0$) leads a very close bound $\gamma_{\max}|_{q=0} = 0.57$ V.

Figure 12 reports the trend of the cumulative energy flow obtained with test signal (36) with $\gamma = \gamma_{\text{exp}} = 0.68$ V. We conclude that the linearized system is compliant with BID conditions with a maximum allowed input amplitude $\gamma_* \in [0.57, 0.68)$ V. Therefore, the computed bound through the proposed approach is at least $\beta = 0.84$ of the exact bound.

E. A Four Stage Amplifier

Here we analyze a basic four stage amplifier circuit in Fig. 13 (see [39, pp. 335-338] for further details). The amplifier is linearized around the operating point

$$U_0 = \begin{bmatrix} V_{\text{CC}} \\ V_{\text{CS}} \\ V_{\text{IN}} \\ V_{\text{OUT}} \end{bmatrix} = \begin{bmatrix} 5 \\ 2 \\ 3.95 \\ 0 \end{bmatrix} \text{V} \tag{45}$$

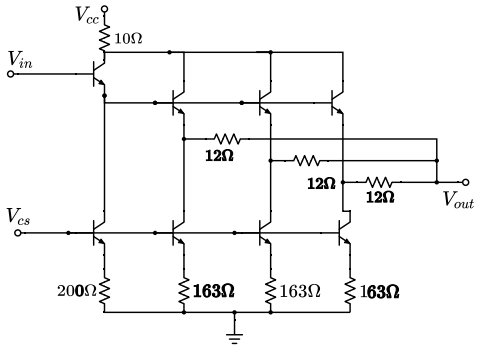

Fig. 13. A four stage amplifier circuit.

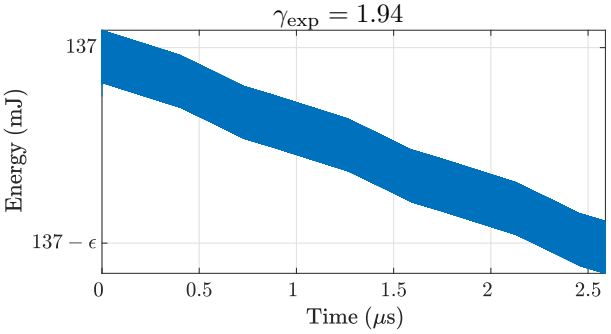

Fig. 14. Cumulative energy flow (as in Fig. 4) for the four-stage amplifier test case.

with corresponding DC steady state outputs

$$Y_0 = I_0 = \begin{bmatrix} I_{\text{CC}} \\ I_{\text{CS}} \\ I_{\text{IN}} \\ I_{\text{OUT}} \end{bmatrix} = \begin{bmatrix} 27.27 \\ 246.2\times10^{-3} \\ 77.10\times10^{-3} \\ 0 \end{bmatrix} \text{mA} \qquad (46)$$

Also in this case a linearized model in form (11) with $n = 40$ states was obtained through a frequency-domain identification based on the vector fitting scheme, applied to the samples of the small-signal frequency response provided by SPICE.

Also for this example the strategy of Sec. VI-1 failed to provide an answer in reasonable time, whereas the other two methods of Sec. VI-2 and Sec. VI-3 provided consistent estimates $\gamma_{\max} = 1.2$ V in 22 s and 149 s, respectively. The estimates for quadratic storage functions ($q = 0$) are the same.

Repetition of the same experimental verification based on the cumulative energy flow analysis with the test signal (36) allows to evaluate the conservatism of the estimates. Transition to a persistently negative energy flow (Fig. 14) occurs for $\gamma_{\text{exp}} = 1.94$ V, which is significantly larger the computed bound $\gamma_{\max}$. Therefore, we can conclude that the exact bound for BID is in the range $\gamma_* \in [1.2, 1.94)$ V, with $\beta = 0.62$.

F. A Low Drop-Out Voltage Regulator

The last test case is a Low Drop-Out (LDO) voltage regulator, whose details and schematic are detailed in [40]. The nominal bias DC inputs are defined as

$$U_0 = \begin{bmatrix} V_{\text{DD}} \\ -I_{\text{L}} \end{bmatrix} = \begin{bmatrix} 1.1\,\text{V} \\ -1.02\,\text{mA} \end{bmatrix}, \quad Y_0 = \begin{bmatrix} I_{\text{DD}} \\ V_{\text{L}} \end{bmatrix} = \begin{bmatrix} 1\,\text{mA} \\ 0.594\,\text{V} \end{bmatrix}$$

where V_{DD} is the the DC voltage applied to Port-1, and I_{L} is the DC current supplied by Port-2. We analyzed the system using a hybrid representation, and we obtain a reduced-order linearized state-space equivalent as in previous examples, through a frequency-domain rational fitting based on the vector fitting scheme. All voltages and currents are normalized with scaling factors $V_{\text{ref}} = 1$ V and $I_{\text{ref}} = 1$ mA.

A total runtime of 3 s and 88 s was required by the two methods of Sec. VI-2 and Sec. VI-3, respectively, to estimate the input bound $\gamma_{\max} = 0.0619$. For a purely quadratic storage function, the predicted bounds are $\gamma_{\max}|_{q=0} = 0.0391$ (method 3) and $\gamma_{\max}|_{q=0} = 0.015$ (method 2).

For this test case, the conditions expressed in Sec. VII-A2 hold, and the bound γ_{exp} can be found analytically for both test signals (35) and (36). The results are

$$\gamma_{\text{exp},1} = 0.0878 \quad \text{and} \quad \gamma_{\text{exp},2} = 0.0621. \qquad (47)$$

The effects of varying γ around $\gamma_{\text{exp},2}$ is llustrated in Fig. 15, confirming the transition from positive to negative cumulative energy flow. We can conclude that the exact bound supporting BID is in the range $\gamma_* \in [0.0619, 0.0621]$. The bound in this case seems to be almost non-conservative, with $\beta = 0.996$.

Table I summarizes all results on BID characterization.

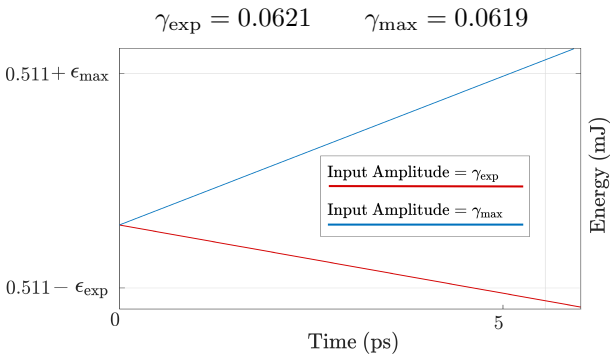

Fig. 15. Cumulative energy flow (as in Fig. 4) for the LDO test case.

TABLE I
SUMMARY OF BID CHARACTERIZATION FOR ALL TEST CASES; $\gamma_{\max}$: COMPUTED UPPER BOUND ON INPUT AMPLITUDE; $\gamma_{\max}|_{q=0}$: SAME, BUT USING A PURE QUADRATIC STORAGE FUNCTION; γ_{exp}: EMPIRICALLY DETERMINED LOWEST INPUT AMPLITUDE FOR WHICH SYSTEM IS NOT BID; $\beta = \gamma_{\max}/\gamma_{\text{exp}}$.

Eaxmple	$\gamma_{\max}$	$\gamma_{\max}\|_{q=0}$	γ_{exp}	β
2^{nd} order circuit	3.53	1.66	4.7	75
Oscillator network	0.43	0.36	0.53	81
Low noise amplifier	0.58	0.58	0.68	84
4-Stage Amplifier	1.2	1.2	1.94	64
LDO	0.0619	0.0391	0.0621	99.6

G. An example of instability induced by BID violation

We conclude this work by providing an example of how the usage of linearized models in a system level simulation may return results that are not only inaccurate, but totally unrealistic, if the proposed BID condition is violated. To this aim, consider an affine linearization of the LDO (Sec. VII-F) around the working point $U_0 = [0.9\text{ V}, -10\ \mu\text{A}]^\top$. We use of this model to simulate the behavior of the circuit reported in

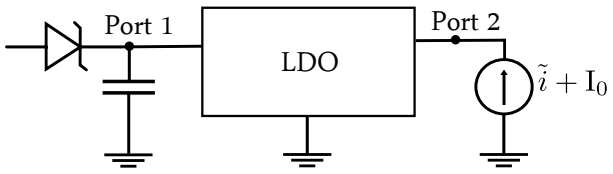

Fig. 16. The LDO device terminated by a reverse current protection circuit and by a load current source.

Fig. 16, where the Port 1 of the regulator is terminated with a reverse current protection diode and a shunt input capacitor. Using reverse current protection diodes is a common practice when dealing with voltage regulators, since inverse current flows, from the output to the input of the device can severely damage the component [41]. These kind of current flows can occur when the output voltage becomes suddenly higher the input voltage. The protection circuit is thought to prevent the reverse current to last in time, by increasing the input voltage of the device and restoring the desired current direction.

A small-signal input disturbance is overimposed to the bias level of the current supplied by the regulator at Port 2. The complete input signal (which violates the BID threshold $\gamma_{\max} = 0.002$) is reported in the top panel of Fig. 17. The middle and bottom panels of Fig. 17 report the voltages at the two device ports, obtained by transient simulation of both the linearized model and the actual LDO circuit.

It is clear that the simulation results are not only inaccurate, but qualitatively different: under the application of this small-signal input, the mean value of the current flow at Port 1 of the model becomes negative and the model continuously supplies power from both of its ports, thus violating the dissipativity condition. Due to the presence of the protection diode, the voltage across the input capacitor ramps up indefinitely. This instability occurs only for the linearized model, since it is able to generate an infinite amount of energy, whereas the actual nonlinear LDO circuit can bear reverse current flows of this type for a finite time before its operating point changes.

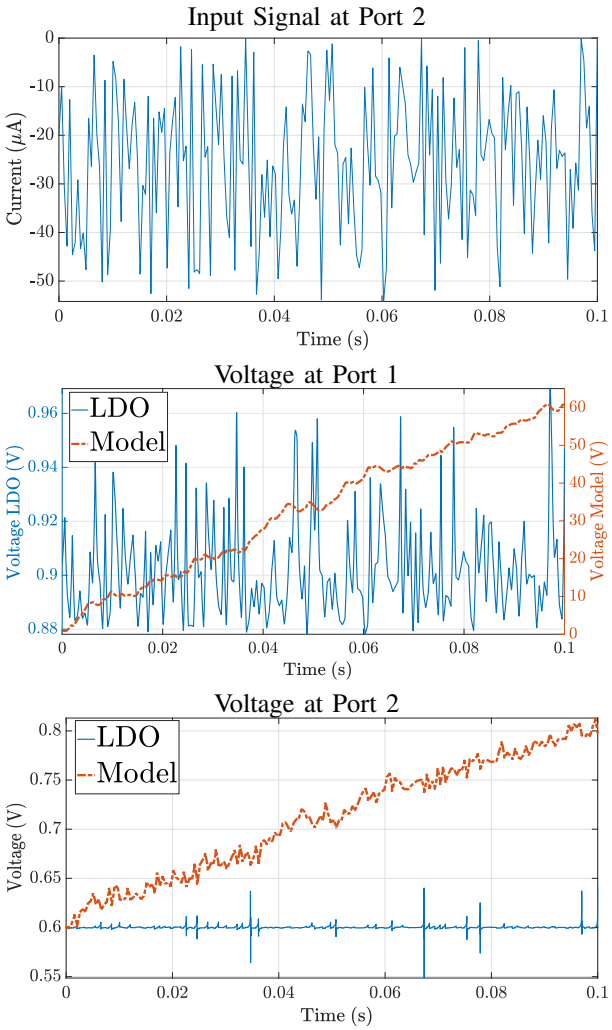

Fig. 17. Simulation of the circuit of Fig. 16. Top panel: input current at Port 2. Middle panel: transient voltage at Port 1 for the transistor level circuit (solid blue) and the affine linearized model (dashed red). Bottom panel: as in middle panel, but for the regulated voltage at Port 2.

VIII. Conclusions

In this work, the new concept of Bounded Input Dissipativity (BID) has been introduced. When applied to linearized models of nonlinear circuit blocks, BID conditions ensure that such models behave as dissipative systems, provided that the small-signal components of the port variables are bounded by some given amplitude γ. In addition to a complete theoretical framework, we have provided a number of algebraic testing methods, which have been applied to various test cases in order to estimate the maximum input amplitude $\gamma_{\max}$ for which the corresponding linearized model behaves as dissipative. It has been shown that this bound should be taken into account whenever a linearized model is exploited to speed up a system level simulation, since its violation can easily lead to unrealistic and nonphysical results.

The BID-preserving input amplitude has been defined here with respect to classical Euclidean norm. This choice has been mainly dictated by simplicity in the development of BID conditions, in particular to obtain a relatively simple characterization of the reachability set and, consequently, efficient numerical verification algorithms. In the future, we will investigate the possibility to extend the same concept to different norms, as required in many applications including analog and mixed signal circuit simulation, where different signals may be subjected to different bounds and ranges of variation, requiring tuning of individual signal components. In addition, future work will address the choice of alternative and more general (non-quadratic) storage functions in order to tighten the estimates for γ and thus reduce the conservatism.

Acknowledgement

The authors thank P. Leite Correia de Toledo for providing the results of the LDO transistor level transient simulations.

References

[1] V. Belevitch, *Classical Network Theory*. Holden-Day, 1968.
[2] M. R. Wohlers, *Lumped and Distributed Passive Networks*. Academic Press, 1969.
[3] B. D. O. Anderson and S. Vongpanitlerd, *Network Analysis and Synthesis*. Prentice-Hall, 1973.

[4] J. C. Willems, "Dissipative dynamical systems part I: General theory," *Archive for Rational Mechanics and Analysis*, vol. 45, no. 5, pp. 321–351, 1972.

[5] ——, "Dissipative dynamical systems part II: Linear systems with quadratic supply rates," *Archive for Rational Mechanics and Analysis*, vol. 45, no. 5, pp. 352–393, 1972.

[6] J. Wyatt, L. Chua, J. Gannett, I. Goknar, and D. Green, "Energy concepts in the state-space theory of nonlinear n-ports: Part I-passivity," *IEEE Trans. Circuits and Syst.*, vol. 28, no. 1, pp. 48–61, 1981.

[7] D. Hill and P. Moylan, "The stability of nonlinear dissipative systems," *IEEE Trans. Autom. Control*, vol. 21, no. 5, pp. 708–711, 1976.

[8] P. Triverio, S. Grivet-Talocia, M. S. Nakhla, F. G. Canavero, and R. Achar, "Stability, causality, and passivity in electrical interconnect models," *IEEE Trans. Advanced Packaging*, vol. 30, no. 4, pp. 795–808, 2007.

[9] S. Grivet-Talocia, "Passivity enforcement via perturbation of Hamiltonian matrices," *IEEE Trans. Circuits Syst. I: Regular Papers*, vol. 51, no. 9, pp. 1755–1769, 2004.

[10] V. Popov, "Absolute stability of nonlinear systems of automatic control," *Autom. Remote Control*, vol. 22, no. 8, pp. 857–875, 1962.

[11] V. Yakubovich, "Solution of some matrix inequalities encountered in the nonlinear control theory," in *Dokl. Akad. Nauk SSSR*, vol. 156, no. 2, 1964, pp. 278–281.

[12] C. Scherer and S. Weiland, *Linear Matrix Inequalities in Control*. Delft, The Netherlands: Dutch Institute for Systems and Control, 2000. [Online]. Available: http://www.st.ewi.tudelft.nl/roos/courses/WI4218/lmi052.pdf

[13] S. Boyd, V. Balakrishnan, and P. Kabamba, "A bisection method for computing the H_∞ norm of a transfer matrix and related problems," *Math. Control, Signals Syst.*, vol. 2, no. 3, pp. 207–219, 1989.

[14] N. Kottenstette, M. J. McCourt, M. Xia, V. Gupta, and P. J. Antsaklis, "On relationships among passivity, positive realness, and dissipativity in linear systems," *Automatica*, vol. 50, no. 4, pp. 1003–1016, 2014.

[15] S. Grivet-Talocia and B. Gustavsen, *Passive Macromodeling: Theory and Applications*. John Wiley & Sons, 2015.

[16] S. Grivet-Talocia, P. Brenner, and F. G. Canavero, "Fast macromodel-based signal integrity assessment for RF and Mixed-Signal modules," in *IEEE International Symposium on Electromagnetic Compatibility*, Honolulu, Hawaii, USA, 2007, pp. 1–6.

[17] S. B. Olivadese, G. Signorini, S. Grivet-Talocia, and P. Brenner, "Parameterized and DC-compliant small-signal macromodels of RF circuit blocks," *IEEE Trans. Components, Packaging and Manufacturing Technology*, vol. 5, no. 4, pp. 508–522, 2015.

[18] T. Bradde, P. Toledo, M. De Stefano, A. Zanco, S. Grivet-Talocia, and P. Crovetti, "Enabling fast power integrity transient analysis through parameterized small-signal macromodels," in *International Symposium on Electromagnetic Compatibility*, Barcelona, Spain, 2019, pp. 759–764.

[19] H. R. Pota and P. J. Moylan, "Stability of locally dissipative interconnected systems," *IEEE Trans. Autom. Control*, vol. 38, no. 2, pp. 308–312, 1993.

[20] H. Zakeri and P. J. Antsaklis, "Local passivity analysis of nonlinear systems: A sum-of-squares optimization approach," in *American Control Conference*, Boston, MA, USA, 2016, pp. 246–251.

[21] ——, "Passivity and passivity indices of nonlinear systems under operational limitations using approximations," *International Journal of Control*, 2020, DOI 10.1080/00207179.2019.1632492.

[22] M. Xia, P. J. Antsaklis, V. Gupta, and F. Zhu, "Passivity and dissipativity analysis of a system and its approximation," *IEEE Trans. Autom. Control*, vol. 62, no. 2, pp. 620–635, 2016.

[23] M. Xia, P. J. Antsaklis, V. Gupta, and M. J. McCourt, "Determining passivity using linearization for systems with feedthrough terms," *IEEE Trans. Autom.Control*, vol. 60, no. 9, pp. 2536–2541, 2014.

[24] S. Sivaranjani, E. Agarwal, and V. Gupta, "Data-driven identification of dissipative linear models for nonlinear systems," *arXiv preprint*, 2019. [Online]. Available: https://arxiv.org/abs/1907.12640

[25] R. E. Kalman and J. E. Bertram, "Control system analysis and design via the "second method" of lyapunov: I—continuous-time systems," *Journal of Basic Engineering*, vol. 82, no. 2, pp. 371–393, 1960.

[26] A. Odabasioglu, M. Celik, and L. T. Pileggi, "PRIMA: Passive reduced-order interconnect macromodeling algorithm," *IEEE Trans. Computer-Aided Design of Integrated Circuits and Systems*, vol. 17, no. 8, pp. 645–654, 1998.

[27] T. Reis and T. Stykel, "Pabtec: Passivity-preserving balanced truncation for electrical circuits," *IEEE Trans. Computer-Aided Design of Integrated Circuits and Systems*, vol. 29, no. 9, pp. 1354–1367, 2010.

[28] B. Gustavsen and A. Semlyen, "Rational approximation of frequency domain responses by vector fitting," *IEEE Trans. Power Delivery*, vol. 14, no. 3, pp. 1052–1061, 1999.

[29] B. Anderson and A. Antoulas, "Rational interpolation and state-variable realizations," *Linear Algebra Appl.*, vol. 137, pp. 479–509, 1990.

[30] L. Ljung, *System Identification: Theory for the User*. Pearson Education, 1998.

[31] G. H. Hines, M. Arcak, and A. K. Packard, "Equilibrium-independent passivity: A new definition and numerical certification," *Automatica*, vol. 47, no. 9, pp. 1949–1956, 2011.

[32] K. Sun, S. Mou, J. Qiu, T. Wang, and H. Gao, "Adaptive fuzzy control for nontriangular structural stochastic switched nonlinear systems with full state constraints," *IEEE Trans. Fuzzy Syst.*, vol. 27, no. 8, pp. 1587–1601, Aug 2019.

[33] J. Qiu, K. Sun, I. J. Rudas, and H. Gao, "Command filter-based adaptive nn control for mimo nonlinear systems with full-state constraints and actuator hysteresis," *IEEE Trans. Cybernetics*, online, DOI 10.1109/TCYB.2019.2944761.

[34] J. Qiu, K. Sun, T. Wang, and H. Gao, "Observer-based fuzzy adaptive event-triggered control for pure-feedback nonlinear systems with prescribed performance," *IEEE Trans. Fuzzy Syst.*, vol. 27, no. 11, pp. 2152–2162, Nov 2019.

[35] S. Boyd, L. El Ghaoui, E. Feron, and V. Balakrishnan, *Linear Matrix Inequalities in System and Control Theory*. SIAM, 1994, vol. 15.

[36] I. Pólik and T. Terlaky, "A survey of the S-lemma," *SIAM Review*, vol. 49, no. 3, pp. 371–418, 2007.

[37] M. Kocvara, "Penlab." [Online]. Available: http://web.mat.bham.ac.uk/kocvara/penlab/

[38] P. Manfredi, D. V. Ginste, D. De Zutter, and F. G. Canavero, "Generalized decoupled polynomial chaos for nonlinear circuits with many random parameters," *IEEE Microwave and Wireless Components Letters*, vol. 25, no. 8, pp. 505–507, 2015.

[39] *Advanced Design System, Examples*, Agilent Technologies, 2011. [Online]. Available: http://edadownload.software.keysight.com/eedl/ads/2011_01/pdf/examples.pdf

[40] T. Y. Man, P. K. Mok, and M. Chan, "A high slew-rate push–pull output amplifier for low-quiescent current low-dropout regulators with transient-response improvement," *IEEE Trans. Circuits Syst. II: Express Briefs*, vol. 54, no. 9, pp. 755–759, 2007.

[41] M. Sellers, "LDO basics: Preventing reverse current." [Online]. Available: https://e2e.ti.com/blogs_/b/powerhouse/archive/2018/07/25/ldo-basics-preventing-reverse-current-in-ldos

APPENDIX

A. Proof of Lemma 1

Proof: By definition of the reachability set, $\tilde{x}(t) = x(t) - X_0 \in R_\gamma$ for any $t \geq 0$. Since $x(\cdot)$ is an absolutely continuous function and $E(\cdot)$ is C^1-smooth, the composition $E(x(\cdot))$ is also absolutely continuous and the derivative exists

$$\frac{d}{dt}E(x(t)) = \frac{\partial E(x(t))}{\partial x}\dot{x}(t) = \\ = \frac{\partial E(x(t))}{\partial x}(Ax(t) + Bu(t)) \overset{(19)}{\leq} u(t)^\top y(t).$$

at almost all $t \geq 0$. The integral inequality (14) is proved now for any input $u \in \mathcal{B}_\gamma^{U_0}$ by integrating the latter inequality. ■

B. Proof of Theorem 1

Proof: Choosing an arbitrary C^1-smooth function $E(x)$ and recalling that $AX_0 + BU_0 = 0$, one notes that

$$\frac{\partial E(X_0)}{\partial x}(AX_0 + BU_0) = 0 < U_0^\top Y_0. \tag{48}$$

Consider now an input $u \in \mathcal{B}_\gamma^{U_0}$ with associated small-signal component $\tilde{u}(t)$. Due to the assumed asymptotic stability, there exist constants κ_x and κ_y such that the small-signal state and

output vectors are bounded as $\|\tilde{x}(t)\|_2 < \kappa_x\gamma$ and $\|\tilde{y}(t)\|_2 < \kappa_y\gamma$ for all t. The power supply can thus be expressed as

$$u(t)^\top y(t) = U_0^\top Y_0 + \mathcal{O}(\kappa_p\gamma), \quad \gamma \to 0^+ \tag{49}$$

for a constant $\kappa_p > 0$. Since E is C^1-smooth with a vanishing time derivative (48) at the equilibrium, it is easy to show that

$$\frac{dE(x(t))}{dt} = \mathcal{O}(\kappa_E\gamma), \quad \gamma \to 0^+ \tag{50}$$

for some constant κ_E. Combining (49) and (50), one shows the existence of some $\gamma_* > 0$ such that the dissipation inequality

$$\frac{dE(x(t))}{dt} < u(t)^\top y(t) \quad \forall t \geq 0 \tag{51}$$

holds $\forall u \in \mathcal{B}_\gamma^{U_0}$ for all $\gamma < \gamma_*$. ■

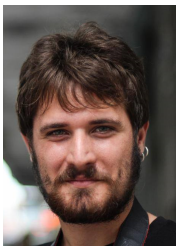

Tommaso Bradde received the Bachelor degree in Electronic Engineering from Roma Tre University, Rome, Italy, in 2015 and the master degree in Mechatronic Engineering at Politecnico di Torino, Turin, Italy, in 2018. He is currently a second-year Ph.D. student in Electrical, Electronics and Communication Engineering within the Politecnico di Torino. His current research is focused on data-driven parameterized macromodeling and its applications to system level power integrity assessments, with the inclusion of active devices. He is co-recipient of the 2018 Best Paper Award of the IEEE International Symposium on Electromagnetic Compatibility and of the Best Student Paper award of the 23rd IEEE wokshop on Signal and Power Integrity.

Stefano Grivet-Talocia (M'98–SM'07–F'18) received the Laurea and Ph.D. degrees in electronic engineering from the Politecnico di Torino, Turin, Italy. From 1994 to 1996, he was with the NASA/-Goddard Space Flight Center, Green- belt, MD, USA. He is currently a Full Professor of electrical engineering with the Politecnico di Torino. He co-founded the academic spinoff company IdemWorks in 2007, serving as the President until its acquisition by CST in 2016. He has authored over 150 journal and conference papers. His current research interests include passive macromodeling of lumped and distributed interconnect structures, model-order reduction, modeling and simulation of fields, circuits, and their interaction, wavelets, time-frequency transforms, and their applications. Dr. Grivet-Talocia was a co-recipient of the 2007 Best Paper Award of the IEEE TRANSACTIONS ON ADVANCED PACKAGING. He received the IBM Shared University Research Award in 2007, 2008, and 2009. He was an Associate Editor of the IEEE TRANSACTIONS ON ELECTROMAGNETIC COMPATIBILITY from 1999 to 2001 and He is currently serving as Associate Editor for the IEEE TRANSACTIONS ON COMPONENTS, PACKAGING AND MANUFACTURING TECHNOLOGY. He was the General Chair of the 20th and 21st IEEE Workshops on Signal and Power Integrity (SPI2016 and SPI2017).

Giuseppe Calafiore is a full professor at DET, Politecnico di Torino, where he coordinates the Systems and Data Science group, and an associate fellow of the IEIIT-CNR. Dr. Calafiore held several visiting positions at international institutions: at the Information Systems Laboratory (ISL), Stanford University, California, in 1995; at the Ecole Nationale Supérieure de Techniques Avancées (ENSTA), Paris, in 1998; and at the University of California at Berkeley, in 1999, 2003, 2007, 2017 and 2018. He was a Senior Fellow at the Institute of Pure and Applied Mathematics (IPAM), University of California at Los Angeles, in 2010. Dr. Calafiore is the author of more than 190 journal and conference proceedings papers, and of eight books. He is a Fellow of the IEEE. He received the IEEE Control System Society "George S. Axelby" Outstanding Paper Award in 2008. His research interests are in the fields of convex optimization, randomized algorithms, identification, and control of uncertain systems, with applications ranging from finance and economic systems to robust control, machine learning, and data science.

Anton Proskurnikov (M'13, SM'18) is an Assistant Professor at the Department of Electronics and Telecommunications, Politecnico di Torino (Italy) and a part-time senior researcher at the Institute for Problems in Mechanical Engineering of the Russian Academy of Sciences. He received the M.Sc. and Ph.D. degrees in applied mathematics from St. Petersburg State University in 2003 and 2005, respectively. He was an assistant professor and senior researcher at St. Petersburg State University (2003-2010), and later a postdoctoral researcher at the University of Groningen (2014-2016) and TU Delft (2016-2018). Anton Proskurnikov is currently serving as Associate Editor at IEEE Transactions on Automatic Control. His research interests include nonlinear dynamics, complex networks, agent-based modeling, robust and nonlinear control.

Zohaib Mahmood received a bachelor of science (B.Sc) degree with honors in electrical engineering in 2007 from the University of Engineering and Technology Lahore. Zohaib continued his education at Massachusetts Institute of Technology (MIT), where he completed dual masters of science (S.M) degrees in electrical engineering & computer science (EECS) and computation for design & optimization (CDO) in 2010 and 2015, respectively, as well as a Ph.D. in EECS in 2015. Since graduating, he has worked for NanoSemi, Inc. in Waltham, MA, where he is working on predistortion based linearization techniques for wireless systems. His research interests include dynamical modeling of linear and nonlinear systems, and application of numerical methods to solve problems of biomedical and telecommunication systems.

Luca Daniel is a Professor of Electrical Engineering and Computer Science at the Massachusetts Institute of Technology. His research interests include development of numerical techniques related to uncertainty quantification, inverse problems, robust optimization, parameterized model order reduction and integral equation solvers. His current applications of interest include evaluating and improving robustness of deep neural networks as well as of magnetic resonance imaging scanners, silicon photonics integrated systems, and electrical power distribution networks. Prof. Daniel has received best-paper awards from several journals of the Institutes of Electrical and Electronics Engineers (IEEE), including Transactions on Power Electronics, Transactions on Computer Aided Design, and Transactions on Components and Manufacturing. He has further received 13 best-paper awards at international conferences. Other honors include the IBM Corporation Faculty Award, the IEEE Early Career Award in Electronic Design Automation, and the Spira Award for Excellence in Teaching from the MIT School of Engineering. Dr. Daniel received best PhD thesis awards from both the Department of Electrical Engineering and Computer Sciences and the Department of Applied Mathematics at the University of California at Berkeley, as well as the Outstanding PhD Dissertation Award in Electronic Design Automation from the Association for Computing Machinery (ACM).